Iterative Demodulation and Decoding of Turbo-Coded M-ary Noncoherent Orthogonal Modulation

Matthew C. Valenti, *Member, IEEE,* and Shi Cheng, *Student Member, IEEE*

***Abstract*—This paper considers bit-interleaved coded modulation (BICM) with a turbo channel code and M-ary orthogonal modulation. The BICM signal is iteratively demodulated and decoded in a noncoherent fashion. A soft demodulator suitable for noncoherent orthogonal modulation is presented, and the convergence of the iterative receiver is analyzed through extrinsic information transfer charts. The demodulator can work either with or without fading amplitude estimates. Extensive simulation results are presented for the well-known cdma-2000 turbo code, and the results are compared with the corresponding channel capacities, which are computed using a Monte Carlo technique. The results indicate gains of up to 1 dB relative to noniterative BICM can be achieved with the iterative receiver.**

***Index Terms*—Bit-interleaved coded modulation (BICM), bit-interleaved coded modulation with iterative decoding (BICM-ID), channel capacity, noncoherent frequency-shift keying (NFSK), orthogonal modulation, turbo codes.**

I. Introduction

THE COMBINATION of orthogonal modulation with noncoherent detection is especially attractive when the phase of the downconverted signal varies significant from symbol-to-symbol. This situation occurs when there is unmitigated frequency offset in the downcoverted signal, high Doppler between transmitter and receiver, or high phase noise in the local oscillators. Examples of applications where such a solution is attractive include military systems using fast frequency hopping [1], communications with high velocity platforms such as missiles, and wireless sensor networks using "cheap" oscillators. As an example of the last application, the IEEE 802.15 Task Group 4 has proposed the use of orthogonal 16-ary modulation with noncoherent detection for low rate wireless personal area networks in the 2.4 GHz ISM band [2]. Since many military systems implement noncoherent orthogonal modulation using noncoherent frequency-shift keying (NFSK), the terms noncoherent orthogonal modulation and NFSK are often used interchangeably.

The capacity of binary NFSK, derived in [3], can be approached to within a decibel in both additive white Gaussian noise (AWGN) and Rayleigh fading by simply using a turbo code [4], [5]. However, binary NFSK is not especially energy efficient. One of the benefits of using orthogonal modulation is that it allows energy-efficiency to be traded off for bandwidth [6]. By using a higher order modulation, the required $\mathcal{E}_b/N_o$ is decreased. In systems that are limited by energy rather than bandwidth (e.g., many military systems and sensor network applications), larger values of M (the number of orthogonal signals in the signal set) are desired.

A pragmatic approach to coding for M-ary modulation with $M > 2$ is *bit-interleaved coded modulation* (BICM) [7]. With BICM, a *binary* channel code is created, bitwised interleaved, and then passed to a M-ary modulator. While slightly inferior to trellis-coded modulation (TCM) in AWGN, BICM is actually superior to TCM in fading because it maximizes the Hamming distance, which is more important than squared-Euclidian distance in fading. With conventional BICM receivers, a demodulator produces soft estimates for each code bit which is then decoded with a standard soft-input decoder. Performance of BICM can be improved by feeding back soft information from the decoder to the demodulator/demapper. The idea of iterating between M-ary demodulation and channel decoding can be traced to several sources, including Benedetto *et al.* [8], ten Brink *et al.* [9], and Li and Ritcey [10], who coined the term *bit-interleaved coded modulation with iterative decoding* (BICM-ID). It is noted that iterative demodulation and decoding has also been successfully applied to other BICM formats that are suitable for noncoherent or differentially-coherent detection, including differential phase-shift keying (DPSK) [11], [12], differential amplitude and phase-shift keying (DAPSK) [13], continuous phase modulation (CPM) [14], and pilot symbol assisted modulation (PSAM) [15], though all of the proposed schemes assume phase stability over at least a few symbols.

The purpose of this paper is to apply the BICM-ID concept to turbo-coded M-ary NFSK. An initial exploration of this concept was presented in [16], which proposed an iterative noncoherent demodulator and turbo decoder for turbo-coded orthogonal modulation. Unfortunately, the one-page limit of the conference proceedings precluded a detailed exposition of the concept. Furthermore, [16] only indicates a performance improvement of 0.1 dB in the waterfall region of the turbo code when using 64-FSK, while our results in Table I show a gain of 0.75 and 1 dB for AWGN and Rayleigh fading for the same modulation order.

The organization and contribution of this paper are as follows. After presenting the system model in Section II, a soft-input soft-output demodulator suitable for noncoherent FSK is described in Section III. The derivation of the demodulator is an extension of the generic *soft mapper* (SOMAP) of Benedetto *et al.* [8]. Explicit formulas are given that are suitable for AWGN channels and Rayleigh-fading channels both with and without fading amplitude estimates. Expressions are given

Manuscript received April 1, 2004; revised January 27, 2005 and March 9, 2005. This work was supported in part by the Xenotran Corporation, Glen Burnie, MD, and Applied Data Trends, Huntsville, AL.

The authors are with the Lane Department of Computer Science and Electrical Engineering, West Virginia University, Morgantown, WV 26506-6109 USA (e-mail: mvalenti@csee.wvu.edu).

Digital Object Identifier 10.1109/JSAC.2005.853794

TABLE I
MINIMUM $\mathcal{E}_b/N_o$ REQUIRED TO ACHIEVE A BER OF 10^{-5} USING THE 6138 BIT cdma2000 TURBO CODE, M-ARY NONCOHERENT FSK, AND EITHER BICM OR THE PROPOSED BICM-ID TECHNIQUE. THE CORRESPONDING SHANNON CAPACITIES AND EXIT THRESHOLDS ARE ALSO GIVEN

			BICM			BICM-ID		
Type	Rate	M	Simulation	Threshold	Capacity	Simulation	Threshold	CM Capacity
AWGN	1/2	2	7.28 dB	7.00 dB	6.71 dB	N/A	N/A	N/A
		4	5.19 dB	4.89 dB	4.65 dB	4.85 dB	4.60 dB	4.18 dB
		16	3.81 dB	3.51 dB	3.28 dB	3.12 dB	2.89 dB	2.07 dB
		64	3.32 dB	2.99 dB	2.81 dB	2.57 dB	2.33 dB	1.11 dB
Rayleigh Fading (CSI)	1/4	2	8.09 dB	7.75 dB	7.40 dB	N/A	N/A	N/A
		4	6.14 dB	5.77 dB	5.39 dB	5.74 dB	5.56 dB	4.88 dB
		16	4.95 dB	4.52 dB	4.20 dB	4.12 dB	3.80 dB	2.80 dB
		64	4.67 dB	4.19 dB	3.89 dB	3.69 dB	3.34 dB	1.85 dB
Rayleigh Fading (NCSI)	1/4	2	8.75 dB	8.43 dB	8.05 dB	N/A	N/A	N/A
		4	6.78 dB	6.42 dB	6.05 dB	6.35 dB	6.01 dB	5.55 dB
		16	5.57 dB	5.13 dB	4.80 dB	4.71 dB	4.40 dB	3.45 dB
		64	5.20 dB	4.74 dB	4.45 dB	4.16 dB	3.94 dB	2.49 dB

in the log-domain, which permits efficient and numerically stable implementation.

The convergence of iterative demodulation and decoding has been considered for convolutionally encoded QAM by ten Brink in [17]. In Section IV, we build upon these results to predict convergence thresholds for turbo-coded NFSK with iterative decoding and demodulation. Part of this convergence analysis involves measuring the mutual information at the output of the soft demodulator, and for certain cases the mutual information at the output of the demodulator coincides with the BICM capacity [7] or the coded modulation (CM) capacity of [3].

In Section V, we present extensive simulation results showing the performance of BICM-ID for M-ary NFSK using the cdma2000 turbo code [18]. We chose this code because it is an accepted standard, has already been optimized, and has a flexible range of code rates. We compare the performance of BICM-ID against that of BICM for all four code rates supported by cdma2000, namely, $R = 1/2$, 1/3, 1/4, and 1/5, and $M = 2$, 4, 16, and 64. We consider the AWGN channel as well as Rayleigh flat-fading both with and without channel state information (CSI). We find that the improvement of using BICM-ID relative to conventional BICM is between 0.34 and 1.04 dB, with the improvement increasing with the modulation order and severity of the channel. Performance is compared against the corresponding thresholds generated in Section IV and the corresponding BICM and CM capacities, which were generated using the Monte Carlo approach suggested by [19] for coherent FSK.

Finally, the paper concludes in Section VI by suggesting paths for future work.

II. SYSTEM MODEL

Before proceeding further, let us stipulate some notational conventions. Bold lowercase letters will be used to denote vectors, e.g., $\mathbf{x}$, and bold uppercase will be used for matrices, e.g., $\mathbf{X}$. All vectors are row-vectors, but can be transposed into column vectors, e.g., $\mathbf{x}^T$. Vector elements are plain lowercase letters with subscripts beginning at zero, e.g., $\mathbf{x} = [x_0, x_1, \ldots, x_{M-1}]$. Matrices are represented as a row of column vectors, e.g., $\mathbf{X} = [\mathbf{x}_0^T, \mathbf{x}_1^T, \ldots, \mathbf{x}_{N-1}^T]$. The function $P(A)$ represents the probability of event A, while $p(x)$ represents a probability density function.

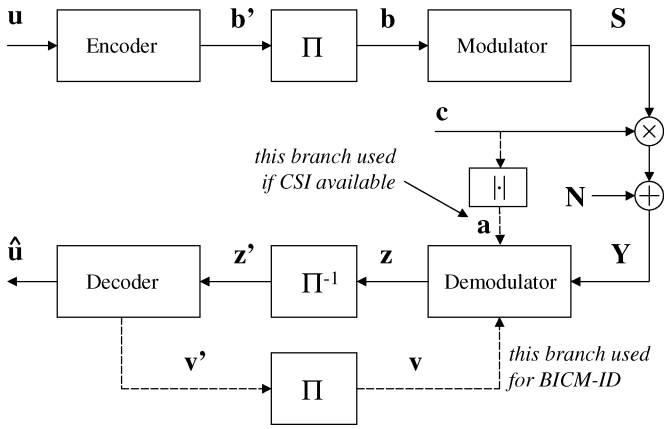

Fig. 1. System model.

A. Transmitter and Channel

The discrete-time system model is shown in Fig. 1. A vector $\mathbf{u} \in \{0,1\}^K$ of message bits is passed through a binary encoder to produce a codeword $\mathbf{b}' \in \{0,1\}^N$, which is interleaved by a permutation matrix $\mathbf{\Pi}$ to produce the bit-interleaved codeword $\mathbf{b} = \mathbf{b}'\mathbf{\Pi}$. The bit-interleaved codeword is then passed through a M-ary orthogonal modulator to produce the $M \times L$ matrix of $L = \lceil N/\log_2 M \rceil$ symbols $\mathbf{S} = [\mathbf{s}_0^T, \ldots, \mathbf{s}_{L-1}^T]$, where the ith symbol $\mathbf{s}_i \in \{\mathbf{e}_0, \ldots, \mathbf{e}_{M-1}\}$ is one of $\mathbf{M}$ possible $\mathbf{M}$-dimensional elementary vectors $\mathbf{e}_m$ comprised of all zeros except for a one in the mth position.

The coded symbol stream passes through a frequency-nonselective channel with complex fading amplitudes $\mathbf{c} \in \mathbb{C}^L$. The ith fading coefficient can be represented as $c_i = a_i \exp\{\theta_i\sqrt{-1}\}$, where a_i and θ_i the real-valued amplitude and phase, respectively. In general, the c_i's could have any distribution, but in the following discussion we focus on two cases: 1) AWGN: $a_i = 1$ and the θ_i's are independent and identically distributed (i.i.d.) uniform and 2) Rayleigh fading: the c_i's are i.i.d. zero-mean complex Gaussian with a variance of 1/2 in each of the real and imaginary directions and, thus, the a_i's are Rayleigh and θ_i's are uniform. The ith fading coefficient c_i is multiplied by the ith symbol $\mathbf{s}_i$ and the result is added with the ith column $\mathbf{n}_i^T$ of the noise matrix $\mathbf{N} \in \mathbb{C}^{M\times L}$, which contains uncorrelated zero-mean complex Gaussian noise samples with variance $\sigma^2 = 1/(2\mathcal{E}_s/N_o)$ in each direction (N_o is the one-sided noise spectral density). The energy per coded symbol $\mathcal{E}_s$ is related to the energy per message bit $\mathcal{E}_b$ by $\mathcal{E}_s = K\mathcal{E}_b/L$. The received complex symbols $\mathbf{Y} = [(c_0\mathbf{s}_0^T + \mathbf{n}_0^T), \ldots, (c_{L-1}\mathbf{s}_{L-1}^T + \mathbf{n}_{L-1}^T)]$ are then passed to the receiver.

B. Receiver

The receiver processes the matrix of received symbols $\mathbf{Y}$ and produces estimates $\hat{\mathbf{u}}$ of the data bits. The receiver is decomposed into a demodulator and a decoder, each of which are implemented using the soft-input soft-output algorithm of [8] and separated by appropriate interleaving/deinterleaving. The demodulator processes the matrix of received symbols $\mathbf{Y}$ to produce extrinsic information $\mathbf{z}$, which is interleaved and passed to the decoder. The demodulator has knowledge of the average symbol signal-to-noise ratio $\mathcal{E}_s/N_o$. While a coherent receiver will have knowledge of the complex fading gains $\mathbf{c}$, the noncoherent receiver will at best only know the fading amplitudes $\mathbf{a} = [a_0, \ldots, a_{L-1}]$. When $\mathbf{a}$ is available, the system is said to have CSI, while when it is not available the system has *no channel state information* (NCSI). Details of the demodulator are discussed in Section III.

The decoder updates the deinterleaved extrinsic information $\mathbf{z}'$, producing new extrinsic information $\mathbf{v}'$ which is interleaved and used by the BICM-ID receiver as *a priori* probability (APP) information. Note that the feedback of extrinsic information from decoder to demodulator is not present in a conventional (feedforward) BICM receiver. The details of the soft-output channel decoder will not be discussed here, as it has already been treated extensively in the literature [8], [20], [21].

The BICM-ID receiver iterates between demodulation and decoding, with the reliability of the exchanged extrinsic information improved after each half-iteration. Note that we have placed no requirements on the type of code. If the code itself does not require iterative decoding, for instance if it is a conventional convolutional code, then it is natural for there to be a single iteration of decoding for every iteration of demodulation. For noniteratively decoded codes, the iterative nature of the BICM-ID receiver substantially increases the complexity of the system, which grows linearly in the number of iterations. For instance, [10] uses a convolutional code and three iterations of BICM-ID decoding, thereby tripling the complexity relative to the noniterative BICM receiver. On the other hand, if the code must be iteratively decoded, BICM-ID does not impose a heavy burden on the overall system complexity. This is because the receiver already must iterate for the sake of decoding and, thus updating the soft demodulator statistics between each decoder iteration is less of a burden than requiring entire iterations solely for the sake of BICM-ID. Complexity can be reduced further by allowing the decoder to execute several local iterations of decoding before updating the soft demodulator metric (this is done in [16] which executes five local iterations of turbo decoding for each of two global iterations of BICM-ID). In our work, we always recompute the demodulator statistics after each turbo-decoding iteration because our goal here is to establish the maximum performance improvement that can be achieved by using BICM-ID. Under our receiver derivation, no error performance benefit is achieved by allowing the decoder to execute several local iterations for each global BICM-ID iteration (a property that we also observed through experimentation).

III. Soft NFSK Demodulator

The soft output demodulator is implemented as a SOMAP, which is described in its most generic form in [8]. The SOMAP works on a symbol-by-symbol basis to compute the likelihoods of each of the μ code bits associated with each received symbol. Let $\mathbf{y}$ denote an arbitrary received symbol and $\mathbf{b} = (b_0, b_1, \ldots, b_{\mu-1})$ denote the μ corresponding code bits. Since the demodulator operates on a symbol-by-symbol basis, we may drop the subscript of $\mathbf{y}$ without introducing any ambiguity. The SOMAP takes input distributions $P(\mathbf{s}; I) = \{P(\mathbf{s} = \mathbf{s}_i; I), 0 \le i \le M-1\}$ and $P(\mathbf{b}; I) = \{P(b_k = q; I), 0 \le k \le \mu - 1, q \in \{0,1\}\}$ and produces output distributions $P(\mathbf{b}; O) = \{P(b_k = q; O), 0 \le k \le \mu - 1, q \in \{0,1\}\}$. While the algorithm in [8] also produces $P(\mathbf{s}; O)$, this output is not needed in this application.

The distributions $P(\mathbf{b}; I)$ and $P(\mathbf{b}; O)$ can be efficiently represented as log-likelihood ratios. In particular, the input distribution $P(\mathbf{b}; I)$ is related to the APP demodulator input by

$$v_k = \log \frac{P(b_k = 1; I)}{P(b_k = 0; I)} \tag{1}$$

while the output distributions $P(\mathbf{b}; O)$ are related to the extrinsic information at the output of the demodulator as

$$z_k = \log \frac{P(b_k = 1; O)}{P(b_k = 0; O)}. \tag{2}$$

The input distribution $P(\mathbf{s}; I)$ is related to the channel observation as

$$P(\mathbf{s} = \mathbf{s}_i; I) = p(\mathbf{y}|\mathbf{s}_i). \tag{3}$$

From [8], the output distribution $P(\mathbf{b}; O)$ is related to the input distributions by

$$P(b_k = q; O) = \sum_{\mathbf{s}_i : b_k(\mathbf{s}_i) = q} P(\mathbf{s} = \mathbf{s}_i; I) \times \prod_{\substack{j=0 \\ j \neq k}}^{\mu-1} P\left(b_j = b_j(\mathbf{s}_i); I\right) \tag{4}$$

$$= \sum_{\mathbf{s}_i : b_k(\mathbf{s}_i)=q} p(\mathbf{y}|\mathbf{s}_i) \prod_{\substack{j=0 \\ j\neq k}}^{\mu-1} \frac{e^{b_j(\mathbf{s}_i)v_j}}{1+e^{v_j}} \quad (5)$$

where the function $b_k(\mathbf{s}_i)$ returns the k^{th} bit associated with the label of $\mathbf{s}_i$ and $P(b_j = b_j(\mathbf{s}_i); I) = e^{b_j(\mathbf{s}_i)v_j}/(1+e^{v_j})$ follows from (1) and the rules of LLR arithmetic [22].

The extrinsic information at the output of the SOMAP can be found in LLR form by substituting (5) into (2), yielding

$$z_k = \log \frac{\sum_{\mathbf{s}_i : b_k(\mathbf{s}_i)=1} p(\mathbf{y}|\mathbf{s}_i) \prod_{\substack{j=0 \\ j\neq k}}^{\mu-1} e^{b_j(\mathbf{s}_i)v_j}}{\sum_{\mathbf{s}_i : b_k(\mathbf{s}_i)=0} p(\mathbf{y}|\mathbf{s}_i) \prod_{\substack{j=0 \\ j\neq k}}^{\mu-1} e^{b_j(\mathbf{s}_i)v_j}}. \quad (6)$$

Note that the $(1+e^{v_j})$ term in (5) cancels in the ratio. This expression can be further simplified by using the *max-star* operator as defined in [21]

$$\max_i * \{x_i\} = \log\left\{\sum_i e^{x_i}\right\} \quad (7)$$

where the pairwise max-star operator is defined as $\max*(x,y) = \max(x,y) + \log(1+e^{-|x-y|}) = \max(x,y) + f_c(|x-y|)$ and multiple arguments imply a recursion of pairwise operations, i.e., $\max*(x,y,z) = \max*(x, \max*(y,z))$. In terms of $\max*$, (6) becomes

$$z_k = \max_{\mathbf{s}_i : b_k(\mathbf{s}_i)=1} * \left[f(\mathbf{y}|\mathbf{s}_i) + \sum_{\substack{j=0 \\ j\neq k}}^{\mu-1} b_j(\mathbf{s}_i)v_j \right] - \max_{\mathbf{s}_i : b_k(\mathbf{s}_i)=0} * \left[f(\mathbf{y}|\mathbf{s}_i) + \sum_{\substack{j=0 \\ j\neq k}}^{\mu-1} b_j(\mathbf{s}_i)v_j \right] \quad (8)$$

where $f(\mathbf{y}|\mathbf{s}_i) = \log p(\mathbf{y}|\mathbf{s}_i) + \kappa$, with κ being any arbitrary constant. Since a conventional BICM demodulator operates without feedback from the decoder, it is implemented using (8) with all $v_j = 0$, or equivalently, with the two summations removed from the expression.

A. Coherent Reception

For a coherent receiver, the complex fading coefficient c is known and, thus, $p(\mathbf{y}|\mathbf{s}_i)$ is conditionally Gaussian [6]

$$p(\mathbf{y}|\mathbf{s}_i) = \left(\frac{\mathcal{E}_s}{\pi N_o}\right)^M \exp\left\{-\frac{\mathcal{E}_s}{N_o}\left[|y_i - c|^2 + \sum_{\substack{j=0 \\ j\neq i}}^{M-1} |y_j|^2\right]\right\}. \quad (9)$$

The quantity $f(\mathbf{y}|\mathbf{s}_i)$ in (8) is found by eliminating terms that are common to all $\mathbf{s}_i$ and taking the log

$$f(\mathbf{y}|\mathbf{s}_i) = \frac{2\mathcal{E}_s}{N_o} \Re\{y_i c^*\} \quad (10)$$

where $\Re\{z\}$ is the real part of z and z^* is the complex-conjugate of z. Thus, the extrinsic information at the output of the SOMAP is found for coherent FSK by substituting (10) into (8).

B. Noncoherent Reception With CSI

For noncoherent reception, the phase θ of c is unknown and thus (9) must be marginalized with respect to θ

$$p(\mathbf{y}|\mathbf{s}_i) = \int_0^{2\pi} p(\theta) \left(\frac{\mathcal{E}_s}{\pi N_o}\right)^M \times \exp\left\{-\frac{\mathcal{E}_s}{N_o}\left[|y_i - a\exp\theta\sqrt{-1}|^2 + \sum_{\substack{j=0 \\ j\neq i}}^{M-1} |y_j|^2\right]\right\} d\theta. \quad (11)$$

Assuming that θ is uniform [6], its pdf is $p(\theta) = 1/(2\pi)$ and

$$p(\mathbf{y}|\mathbf{s}_i) = \left(\frac{\mathcal{E}_s}{\pi N_o}\right)^M \exp\left\{-\frac{\mathcal{E}_s}{N_o}\left[a^2 + \sum_{j=0}^{M-1} |y_j|^2\right]\right\} \times I_0\left(\frac{2\mathcal{E}_s a|y_i|}{N_o}\right) \quad (12)$$

where $I_0(\cdot)$ is the zeroth-order modified Bessel function of the first kind. Since all terms that are not inside the Bessel function are common to all $\mathbf{s}_i$

$$f(\mathbf{y}|\mathbf{s}_i) = \log I_0\left(\frac{2\mathcal{E}_s a|y_i|}{N_o}\right). \quad (13)$$

Thus, the extrinsic information at the output of the SOMAP is found for noncoherent FSK with CSI by substituting (13) into (8). Note that the logarithm and Bessel function always appear together as $\log[I_o(\cdot)]$ and so this combined function can be implemented as a single table lookup. A piecewise linear approximation for this nonlinear function is given in [4].

C. Noncoherent Reception Without CSI

If the fading amplitude a is not known, but its pdf $p(a)$ is, then (12) must be marginalized with respect to $p(a)$

$$p(\mathbf{y}|\mathbf{s}_i) = \int_0^{\infty} p(a) \left(\frac{\mathcal{E}_s}{\pi N_o}\right)^M \exp\left\{-\frac{\mathcal{E}_s}{N_o}\left[a^2 + \sum_{j=0}^{M-1} |y_j|^2\right]\right\} \times I_0\left(\frac{2\mathcal{E}_s a|y_i|}{N_o}\right) da. \quad (14)$$

If a is Rayleigh, then [5]

$$p(\mathbf{y}|\mathbf{s}_i) = \left(\frac{1}{1+\frac{\mathcal{E}_s}{N_o}}\right) \left(\frac{\mathcal{E}_s}{\pi N_o}\right)^M \exp\left\{-\frac{\mathcal{E}_s}{N_o} \sum_{j=0}^{M-1} |y_j|^2\right\} \times \exp\left\{\frac{\left(\frac{\mathcal{E}_s}{N_o}\right)^2 |y_i|^2}{1+\frac{\mathcal{E}_s}{N_o}}\right\}. \quad (15)$$

Since all terms except the rightmost exponential cancel out in the probability ratio

$$f(\mathbf{y}|\mathbf{s}_i) = \frac{\left(\frac{\mathcal{E}_s}{N_o}\right)^2 |y_i|^2}{1+\frac{\mathcal{E}_s}{N_o}}. \quad (16)$$

Thus, the extrinsic information at the output of the SOMAP is found for noncoherent FSK without CSI by substituting (16) into (8).

IV. Convergence and Capacity Analysis

As is common for turbo-coded systems, the bit-error rate (BER) curves for the proposed system are characterized by a sharp transition from a high error rate region to a low error rate floor. The location of this transition, also called the *turbo-cliff* or *waterfall* region, can be predicted using an extrinsic information transfer (EXIT) chart [17], [23].

The starting point of the convergence analysis is a characterization of mutual information at the output of the soft demapper as a function of the channel SNR and the mutual information of the *a priori* information passed to the demodulator from the decoder. In terms of our notation, the bitwise mutual information at the output of a soft demapper can be expressed as [17]

$$I_{\mathbf{z}} = 1 - \frac{1}{\mu}\sum_{k=0}^{\mu-1} E\left[\log_2 \frac{P(b_k=0;O)+P(b_k=1;O)}{P(b_k=q;O)}\right] \tag{17}$$

where the expectation is over the two equally likely values of $b_k = q \in \{0,1\}$, the received signal $\mathbf{y}$ when the channel SNR is $\mathcal{E}_s/N_o$, and the *a priori* input $\mathbf{v}$ when the mutual information of the *a priori* input is $I_{\mathbf{v}}$.

Given the complexity of the demmapper, direct evaluation of (17) is not generally feasible. However, it can be accurately evaluated using a Monte Carlo approach, which proceeds as follows. First a symbol $\mathbf{s}$ is randomly chosen from the signal set. The symbol is multiplied by a random complex channel gain c and added with complex Gaussian noise with variance $1/(2\mathcal{E}_s/N_o)$. The received symbol $\mathbf{y}$ is passed into the demodulator along with a randomly generated APP input $\mathbf{v}$. The input $\mathbf{v}$ is Gaussian distributed and has mutual information $I_{\mathbf{v}}$ and variance σ_v^2. The mean of v_k is $\sigma_v^2/2$ when $b_k = 1$ and $-\sigma_v^2/2$ when $b_k = 0$. Histograms of several decoding runs confirmed that this APP input was indeed Gaussian distributed. The demodulator inputs are processed using (8) and the resulting μ bitwise extrinsic information values $\mathbf{z}$ are stored. For each value of $\mathcal{E}_s/N_o$ and $I_{\mathbf{v}}$, this processes is repeated a large number of times and the stored values of $\mathbf{z}$ are used to calculate the output mutual information. The exact expression for output mutual information is obtained by substituting identities (2) and (7) into (17) and noting that $b_k = q \in \{0,1\}$ are equally likely, yielding

$$I_{\mathbf{z}} = 1 - \frac{\log_2(e)}{\mu}\sum_{k=0}^{\mu-1} E\left[\max\nolimits*\left(0, z_k(-1)^{b_k(\mathbf{s})}\right)\right]. \tag{18}$$

Some example extrinsic transfer characteristics are shown for the proposed soft demodulator in Fig. 2 for $M = 4$, 16, and 64 in an AWGN channel with $\mathcal{E}_s/N_o = 3$ dB. The x axis shows the mutual information $I_{\mathbf{v}}$ of the APP input, while the y axis shows the corresponding mutual information $I_{\mathbf{z}}$ at the demodulator output. The conventional BICM receiver corresponds to the case that no information is fed back from the decoder and, hence, $I_{\mathbf{v}} = 0$. In fact, the value of $I_{\mathbf{z}}$ when $I_{\mathbf{v}} = 0$ corresponds the the BICM capacity [7]. On the other hand, when $I_{\mathbf{v}} = 1$ the demodulator has full knowledge of all the bits in the symbol *except* for bit b_k. In this case, the demodulation boils down to a binary decision and, hence, the value of $I_{\mathbf{z}}$ when $I_{\mathbf{v}} = 1$ corresponds to the capacity of binary NFSK. Another interesting observation is that the value of $I_{\mathbf{z}}$ when $I_{\mathbf{v}} = 1/2$ corresponds to the CM capacity [7], , as indicated on the figure by the dashed lines.

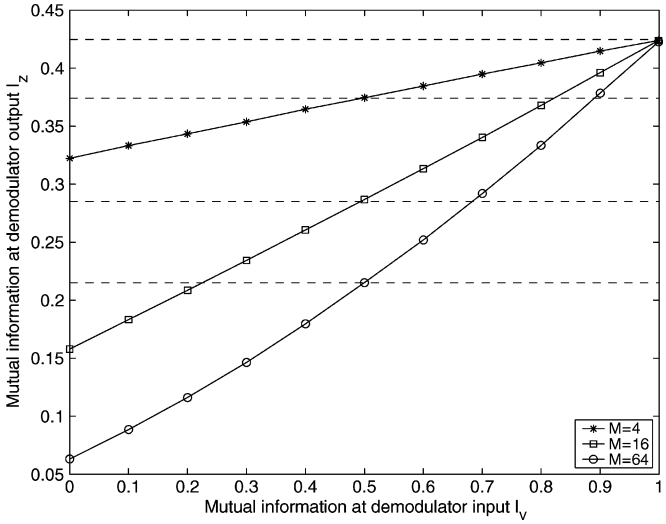

Fig. 2. Extrinsic information transfer characteristics for soft NFSK demodulator in AWGN at $\mathcal{E}_s/N_o = 3$ dB for several values of M. Also shown (dashed lines) is the CM capacity [3] of $M = \{2, 4, 16, 64\}$.

Next, the influence of the channel decoder must be taken into account. This is complicated by two factors. First, while we have observed that the output of the channel decoder (APP input to the demodulator) was Gaussian distributed, the output of the soft demodulator was highly non-Gaussian. Histograms of the demodulator output (not shown) reveal that it is nonsymmetric and very "peaky" over a wide range of channel conditions (even when the channel is AWGN). This is due to a combination of the nonlinear operations within the demodulator, such as (13) or (16), and the fact that each output z_k only depends on a single noisy observation $\mathbf{y}$ and a small number $(\mu - 1)$ of APP inputs and, therefore, the Central Limit Theorem does not hold. The second complicating factor is that we are using a turbo code and, therefore, the iterative nature of the channel decoder must be considered. Both of these factors were taken into account by carefully generating the extrinsic transfer characteristic of the turbo decoder.

In contrast with [17] and [23], we did not completely separate the generation of the decoder's extrinsic transfer characteristic from the demodulator's characteristic, since this would require an assumption regarding the distribution of the decoder's input. Instead, the generation of the decoder characteristic was linked to the demodulator's characteristic as follows. First the demodulator characteristic is plotted for the desired value of $\mathcal{E}_s/N_o$. An example for $M = 16$ in Rayleigh fading with CSI and $\mathcal{E}_s/N_o = 4$ dB is shown in Fig. 3. Then, for each value of demodulator input extrinsic information $I_{\mathbf{v}}$, the demodulator characteristic curve is used to determine the mutual information $I_{\mathbf{z}}$ at the demodulator output. Rather than passing Gaussian distributed extrinsic information with mutual information $I_{\mathbf{z}'} = I_{\mathbf{z}}$ into the decoder, the actual demodulator was simulated with Gaussian distributed input extrinsic information $I_{\mathbf{v}}$ to assure that the input to the decoder will have the correct distribution. Given the actual demodulator outputs, the mutual information at the decoder output $I_{\mathbf{v}'}$ was tracked by simulating entire turbo codewords and

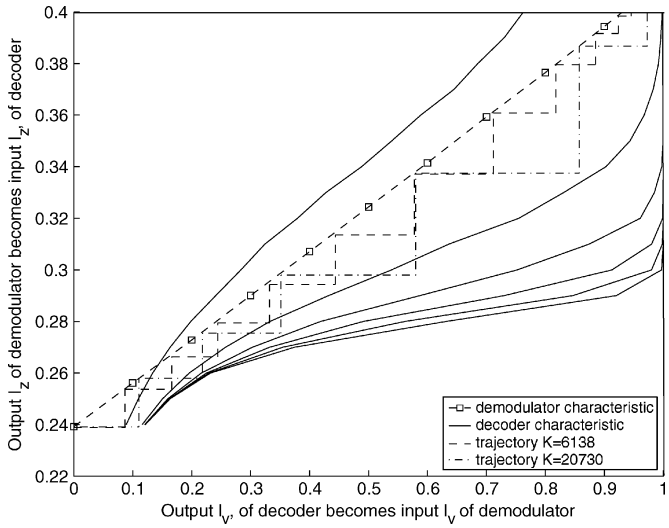

Fig. 3. EXIT chart for BICM-ID using $M = 16$ NFSK and the rate $R = 1/4$ cdma2000 turbo code in Rayleigh fading with CSI at $\mathcal{E}_b/N_o = 4$ dB. Two average decoding trajectories are shown: the narrower trajectory is for a $K = 6138$ bit interleaver and one local channel decoding iteration per global iteration, and the wider trajectory is for a $K = 20\,730$ bit interleaver and two local channel decoding iterations per global iteration.

measuring the output mutual information after each decoder iteration. This process is repeated for a large number of NFSK modulated turbo codewords, and the resulting average decoder output mutual information $I_{\mathbf{v}'}$ is plotted for each iteration on the EXIT chart against the value of the demodulator's output extrinsic information $I_{\mathbf{z}}$. The example shown in Fig. 3 corresponds to the rate $R = K/N = 1/4$ cdma2000 turbo code[1] and channel decoding iterations one through six (there is little change in the curves for iterations beyond six, especially, in the pinch-off regions that most affect convergence). Note that since $M = 16$ and $R = 1/4$, $\mathcal{E}_s/N_o = \mathcal{E}_b/N_o$. While a decoder characteristic generated in this way will depend on the interleaver length K, we found that the characteristics for $K = 6138$ and $K = 20\,730$ were nearly identical.

Generating the decoder characteristic in this manner is not equivalent to simply letting the BICM-ID receiver run freely, since we are holding the value of input/output mutual information at the demodulator constant, while in the BICM-ID receiver this value will increase after each iteration. Because the demodulator's extrinsic information is carefully controlled, the EXIT chart can be used to glean some insight into the convergence behavior of the complete BICM-ID receiver. The EXIT chart is read by first initializing demodulator input $I_{\mathbf{v}} = 0$. Next, the initial value at the output of the demodulator $I_{\mathbf{z}}$ is read off the chart. Assume that there is one local channel decoding iteration for every global BICM-ID iteration. In this case, the output of the decoder $I_{\mathbf{v}'}$ after the first BICM-ID iteration is the intersection of the horizontal line $I_{\mathbf{z}'} = I_{\mathbf{z}}$ and the decoder characteristic corresponding to decoder iteration one. Next, the output of the demodulator $I_{\mathbf{z}}$ during the second iteration is found as the intersection of the vertical line $I_{\mathbf{v}'} = I_{\mathbf{v}}$ and the demodulator's characteristic. The output of the decoder after the second iteration is found like it was for the first iteration, only now the characteristic for decoder iteration two is used. The trajectory continues in a zig-zag fashion, bouncing between the demodulator characteristic and the characteristic of the decoder for the corresponding iteration number. If the zig-zag path is able to progress to the right side of the EXIT chart, then decoding will succeed with high probability, indicating that system is operating with $\mathcal{E}_b/N_o$ greater than the threshold. Conversely, if the path gets stuck at some $I_{\mathbf{v}} < 1$, then decoding is likely to fail, indicating that the system is operating with $\mathcal{E}_b/N_o$ smaller than the threshold. The threshold itself is found by determining the minimum value of $\mathcal{E}_b/N_o$ for which the path progresses all the way to the right side of the chart.

The effectiveness of the EXIT chart can be illustrated by overlaying actual decoding trajectories for the rate $R = 1/4$ cdma2000 turbo code on Fig. 3. The trajectories are obtained by simulating the entire BICM-ID receiver and measuring the appropriate mutual information after each iteration. Fig. 3 shows two average trajectories, the first of which (dotted line) is for an interleaver length of $K = 6138$. At first, the trajectory bounces between the demodulator characteristic and the decoder characteristic corresponding to the same iteration. While the trajectory is always bounded by the demodulator characteristic, for higher iterations it no longer touches the appropriate decoder characteristic. This is due to two reasons. First, a length $K = 6138$ interleaver is too short for the EXIT chart to be exact and causes correlations to arise in the actual BICM-ID receiver that are not accounted for in the EXIT analysis. Second, while the first constituent channel decoder receives extrinsic information from the demodulator due to iteration n, the (local) extrinsic information that it receives from the other constituent decoder actually corresponds to iteration $n - 1$. Thus, when performing one local channel iteration per global BICM-ID iteration, the mutual information at the output of the decoder does not reach the decoder characteristic curve for iterations n. These two effects can be visualized by showing the average trajectory with a larger interleaver (in this case, $K = 20\,730$) and performing *two* local iterations per global iteration. This is the second trajectory shown in Fig. 3, and it can be seen that under these conditions the trajectory follows the EXIT chart more closely, though still not perfectly. Note that while the trajectory of later iterations do not follow the decoder characteristic exactly, it is the trajectory for the first few iterations that most influence the pinch-off region [23], and it is in this region that the EXIT curve is most closely followed. The accuracy of the EXIT analysis is confirmed in the next section by comparing the predicted thresholds against the location of the waterfall found through simulation.

V. Simulation Results

To illustrate the effectiveness of the proposed BICM-ID technique for M-ary NFSK, we conducted an extensive set of simulations using the turbo code from the cdma2000 specification [18]. We investigated all four code rates supported by cdma2000, specifically $R = 1/2$, 1/3, 1/4, and 1/5. While

[1]The cdma2000 turbo code uses a pair of rate 1/3 recursive systematic convolutional constituent codes with generators $[1, (1 + D + D^3)/(1 + D^2 + D^3), (1 + D + D^2 + D^3)/(1 + D^2 + D^3)]$. The unpunctured rate of the code is 1/5. Rate 1/4 is achieved by puncturing every other bit in the second parity stream; rate 1/3 is achieved by puncturing the entire second parity stream; rate 1/2 is achieved by puncturing the entire second parity stream and every other bit in the first parity stream [18].

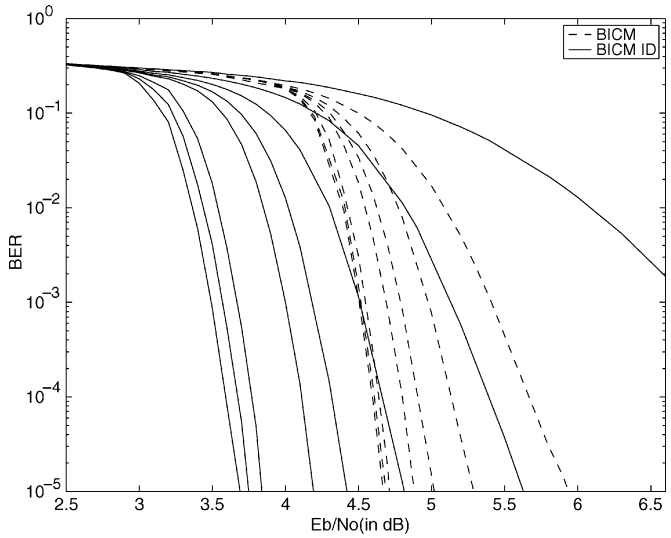

Fig. 4. BER performance in Rayleigh fading (*with* CSI) of the $R = 1/4$ input-length $K = 6138$ bit cdma2000 turbo code using 64-ary NFSK and both BICM (dashed line) and BICM-ID (solid line). From right to left, the curves show performance after 1, 2, 3, 4, 5, 10, 16, and 30 iterations.

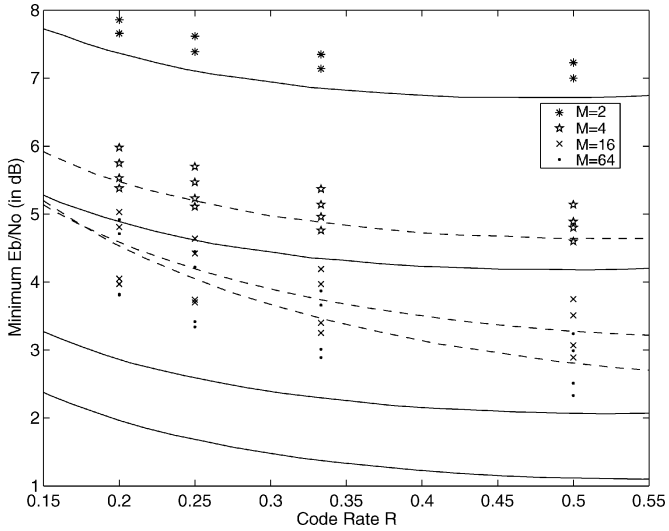

Fig. 5. Minimum $\mathcal{E}_b/N_o$ required to achieve $\mathrm{BER} = 10^{-4}$ and thresholds predicted by EXIT analysis as a function of code rate R over an AWGN channel using M-ary NFSK modulation and the $K = 6138$ bit cdma2000 turbo code. For $M = 2$ two points are shown: the upper point is the simulated value and the lower point is the EXIT threshold. For $M = \{4, 16, 64\}$ four points are shown, from top to bottom: 1) simulated BICM receiver; 2) threshold for BICM; 3) simulated BICM-ID receiver; and 4) threshold for BICM-ID. For reference, the corresponding BICM [7] (dashed) and CM [3] (solid) capacities are shown.

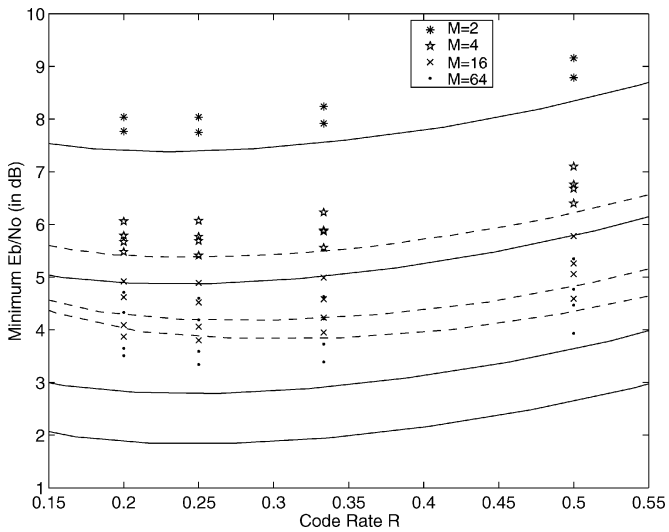

Fig. 6. Minimum $\mathcal{E}_b/N_o$ for a fully interleaved Rayleigh flat-fading channel using M-ary NFSK modulation and CSI. See caption to Fig. 5 for full description.

cdma2000 supports 12 distinct frame sizes, we focused on frames created using $K = 6138$ message bits (we also tested the three larger frame sizes of 9210, 12 282, and 20 730, but found that their performance was not significantly better). The BICM interleaver $\boldsymbol{\Pi}$ was implemented as a μ by L block interleaver, with bits written into the interleaver row-wise and read out column-wise. We also tried some other interleaver designs, including s-random interleavers and interleavers designed according to the three rules in [24]. However, we found that performance was not significantly influenced by interleaver design, presumably due to the fact that the turbo code already contains its own internal interleaver.

For each code rate, we considered AWGN, as well as fully interleaved Rayleigh flat-fading both with and without CSI. In all cases, it is assumed that the average value of $\mathcal{E}_b/N_o$ is known at the receiver. Four values of the modulation order M were considered, $M = 2$, 4, 16, and 64. For $M > 2$, both BICM and BICM-ID were considered (for $M = 2$, BICM-ID degenerates into BICM and thus separate results are not necessary). In each case, 30 iterations of BICM-ID decoding were performed (with a single local iteration of turbo decoding for each global iteration of BICM-ID). For every data point, the simulation ran until at least 30 frame errors were recorded.

BER curves for both BICM (dashed lines) and BICM-ID (solid lines) are shown for Rayleigh fading with CSI, $M = 64$, and $R = 1/4$ in Fig. 4. From right to left, the performance after iterations 1, 2, 3, 4, 5, 10, 16, and 30 are shown. The curves indicate that the performance of BICM-ID after 4 iterations is always better than the performance of BICM after all 30 iterations. This implies that, although BICM-ID is marginally more complex per iteration than BICM, a system using BICM-ID can actually be much less complex than BICM because it can achieve the same performance by running fewer iterations.

BER curves for the other simulated scenarios exhibited similar behavior. Since space does not permit BER curves to be shown for all 84 scenarios, we instead found for each case the value of $\mathcal{E}_b/N_o$ for which the $\mathrm{BER} = 10^{-4}$. These values are indicated in Figs. 5–7. In particular, the value of $\mathcal{E}_b/N_o$ is shown as a function of code rate R for all four modulation orders in AWGN (Fig. 5), Rayleigh fading with CSI (Fig. 6), and Rayleigh fading with NCSI (Fig. 7). The thresholds found using the convergence analysis of Section IV are also indicated. For each value of $M > 2$, four points are shown. From top to bottom these points correspond to: 1) simulated BICM receiver; 2) threshold for BICM; 3) simulated BICM-ID receiver; and 4) threshold for BICM-ID. For reference, the corresponding BICM [7] and CM [3] capacities are shown.

Due to the noncoherent combining penalty [3], performance does not necessarily improve with decreasing code rate as it does

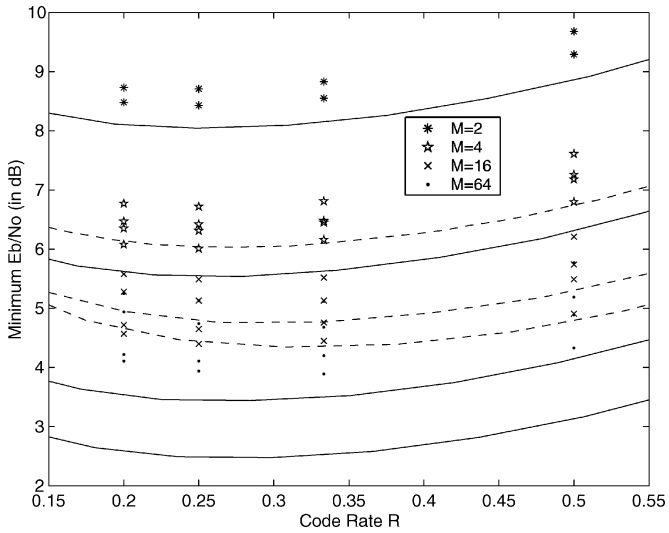

Fig. 7. Minimum $\mathcal{E}_b/N_o$ for a fully interleaved Rayleigh flat-fading channel using M-ary NFSK modulation and *no* CSI. See caption to Fig. 5 for full description.

for coherent modulation. Thus, for each channel type and modulation order there is an optimal value of R; decreasing R below this value actually increases the required $\mathcal{E}_b/N_o$. For AWGN, $R = 1/2$ performed best, while in both Rayleigh-fading scenarios, $R = 1/4$ was best. In Table I, we list the value of $\mathcal{E}_b/N_o$ required to achieve a BER of 10^{-5} for each channel type and modulation order using the cdma2000 code rate with the best performance. For each case, the table lists the $\mathcal{E}_b/N_o$ for both BICM and BICM-ID along with the corresponding thresholds and capacities. In fading, the penalty for not using CSI is about 0.6 dB in all cases. The decibel gain of BICM-ID over BICM increases with M, with gains between 0.34 and 0.43 dB for $M = 4$, between 0.69 and 0.86 dB for $M = 16$, and between 0.75 and 1.04 dB for $M = 64$. The gain in fading was higher than the gain in AWGN. While the observed performance actually exceeded the BICM capacity, there is still a gap to the CM capacity, and this gap increases with M, suggesting that further improvements to this process are possible. The threshold for BICM-ID predicted by EXIT analysis are between 0.18 and 0.35 dB lower than the simulated results, indicating that the analysis is a good indicator of the location of the turbo cliff.

VI. Conclusion

Noncoherent communications using orthogonal modulation is a natural choice when there is little phase coherence from symbol to symbol. Orthogonal modulation also has the attractive feature of allowing bandwidth to be traded for improved energy efficiency, making it an appealing alternative in energy-limited channels. While binary turbo codes are effective for binary modulation formats, special care should be taken when dealing with M-ary modulation. In particular, the demodulator should use *a priori* information derived from the decoder. While the concept of iterative demodulation and decoding can be applied to any M-ary modulation, in this paper we have focused on the application to noncoherent orthogonal modulation, giving an explicit formulation for the soft demodulator. Our results have shown that a gain of about 1 dB can be attained by properly exploiting the extrinsic information fed back from the decoder. EXIT analysis [17] can be used to accurately predict the decoding threshold, though special care needs to be taken when generating the decoder characteristic.

In this paper, it is assumed that the average $\mathcal{E}_b/N_o$ is known at the receiver, and that a perfect automatic gain control (AGC) unit is able to appropriately normalize the signal. However, in the absence of a perfect AGC, $\mathcal{E}_b$ and N_o need to be estimated separately [1], which is nontrivial for NFSK and a topic for future work [27]. Likewise, our results for Rayleigh fading with CSI assumed that the amplitude estimates can be perfectly estimated. While this is difficult when the channel coherence time is short, accurate estimates can be achieved if the amplitude's coherence time is sufficiently long by periodically transmitting pilot symbols or tones [26]. A more sophisticated blind receiver could actually switch between operating in NCSI mode and CSI mode. During the first few iterations, the receiver does not know the fading amplitudes and must operate without CSI. However, as the decoder begins to resolve the data, the fading amplitudes could be estimated. Then, the estimated fading amplitudes could provide CSI for future iterations. A hybrid receiver could operate in NCSI mode for some symbols and CSI mode for only those symbols whose amplitudes have been reliably estimated. Finally, we note that iterative demodulation and decoding could be used for noncoherent MIMO communications, for instance, the modulation proposed in [26], which generalizes noncoherent orthogonal modulation for multi-antenna transmission systems.

Acknowledgment

The authors would like to thank Dr. M. McCloud, Dr. D. Torrieri, and the anonymous reviewers for their valuable comments regarding this paper.

References

[1] D. Torrieri, *Principles of Spread-Spectrum Communication Systems*. New York: Springer-Verlag, 2004.

[2] *Draft Standard for Part 15.4: Wireless Medium Access Control (MAC) and Physical Layer (PHY) Specifications for Low Rate Wireless Personal Area Networks (LR-WPAN's)*, LAN/MAN Standards Committee of the IEEE Computer Society, Draft P802.15.4/D18, Feb. 2003.

[3] W. E. Stark, "Capacity and cutoff rate of noncoherent FSK with nonselective Rician fading," *IEEE Trans. Commun.*, vol. COM–33, no. 11, pp. 1153–1159, Nov. 1985.

[4] E. K. Hall and S. G. Wilson, "Turbo codes for noncoherent channels," in *Proc. IEEE GLOBECOM, Commun. Theory Mini-Conf.*, Phoenix, AZ, Nov. 1997, pp. 66–70.

[5] A. Ramesh, A. Chockalingam, and L. B. Milstein, "Performance of noncoherent turbo detection on Rayleigh-fading channels," *Proc. IEEE Global Telecommun. Conf. (GLOBECOM)*, pp. 1193–1198, Nov. 2001.

[6] J. Proakis, *Digital Communications*, 4th ed. New York: McGraw-Hill, 2001.

[7] G. Caire, G. Taricco, and E. Biglieri, "Bit-interleaved coded modulation," *IEEE Trans. Inf. Theory*, vol. 44, no. 3, pp. 927–946, May 1998.

[8] S. Benedetto, G. Montorsi, D. Divsalar, and F. Pollara, "Soft-input soft-output modules for the construction and distributed iterative decoding of code networks," *Eur. Trans. Telecommun.*, vol. 9, pp. 155–172, Mar.–Apr. 1998.

[9] S. ten Brink, J. Speidel, and R.-H. Yan, "Iterative demapping and decoding for multilevel modulation," in *Proc. IEEE Global Telecommun. Conf. (GLOBECOM)*, Sydney, Australia, Nov. 1998, pp. 579–584.

[10] X. Li and J. A. Ritcey, "Bit-interleaved coded modulation with iterative decoding," *IEEE Commun. Lett.*, vol. 1, no. 1, pp. 169–171, Nov. 1997.

[11] P. Hoeher and J. Lodge, "Turbo DPSK: Iterative differential PSK demodulation and channel decoding," *IEEE Trans. Commun.*, vol. 47, no. 6, pp. 837–843, Jun. 1999.

[12] I. Marsland and P. Mathiopoulos, "On the performance of iterative noncoherent detection of coded M-PSK signals," *IEEE Trans. Commun.*, vol. 48, no. 4, pp. 588–596, Apr. 2000.
[13] L.-J. Lampe and R. Schober, "Low-complexity iterative demodulation for noncoherent coded transmission over Ricean-fading channels," *IEEE Trans. Veh. Technol.*, vol. 50, no. 6, pp. 1481–1496, Nov. 2001.
[14] K. Narayanan and G. Stuber, "Performance of trellis-coded CPM with iterative demodulation and decoding," *IEEE Trans. Commun.*, vol. 49, no. 4, pp. 676–687, Apr. 2001.
[15] M. C. Valenti and B. D. Woerner, "Iterative channel estimation and decoding of pilot symbol assisted turbo codes over flat-fading channels," *IEEE J. Sel. Areas Commun.*, vol. 19, no. 9, pp. 1697–1705, Sep. 2001.
[16] P. C. P. Liang and W. E. Stark, "Algorithm for joint decoding of turbo codes and M-ary orthogonal modulation," in *Proc. IEEE Int. Symp. Inf. Theory (ISIT)*, Sorrento, Italy, Jun. 2000, p. 191.
[17] S. ten Brink, "Convergence of iterative decoding," *Electron. Lett.*, vol. 35, pp. 806–808, May 13, 1999.
[18] *Physical Layer Standard for cdma2000 Spread-Spectrum Systems, Release C*, Third Generation Partnership Project 2 (3GPP2), 3GPP2 C.S0002-C Version 1.0, May 28, 2002.
[19] S. J. MacMullan and O. M. Collins, "The capacity of orthogonal and biorthogonal codes on the Gaussian channel," *IEEE Trans. Inf. Theory*, vol. 44, pp. 1217–1232, May 1998.
[20] P. Robertson, P. Hoeher, and E. Villebrun, "Optimal and suboptimal maximum *a posteriori* algorithms suitable for turbo decoding," *Eur. Trans. Telecommun.*, vol. 8, no. 2, pp. 119–125, Mar./Apr. 1997.
[21] A. J. Viterbi, "An intuitive justification and a simplified implementation of the MAP decoder for convolutional codes," *IEEE J. Sel. Areas Commun.*, vol. 16, no. 2, pp. 260–264, Feb. 1998.
[22] J. Hagenauer, E. Offer, and L. Papke, "Iterative decoding of binary block and convolutional codes," *IEEE Trans. Commun.*, vol. 42, no. 2, pp. 429–445, Mar. 1996.
[23] S. ten Brink, "Convergence behavior of iteratively decoded parallel concatenated codes," *IEEE Trans. Commun.*, vol. 49, no. 10, pp. 1727–1737, Oct. 2001.
[24] X. Li, A. Chindapol, and J. A. Ritcey, "Bit-interleaved coded modulation with iterative decoding and 8-PSK signaling," *IEEE Trans. Commun.*, vol. 50, no. 8, pp. 1250–1257, Aug. 2002.
[25] J. K. Cavers, "An analysis of pilot symbol assisted modulation for Rayleigh-fading channels," *IEEE Trans. Veh. Technol.*, vol. 40, no. 4, pp. 686–693, Nov. 1991.
[26] M. L. McCloud, "Layered signals for use on the noncoherent MIMO block fading channel," in *Proc. Allerton Conf. Commun., Control, Computing*, Nov. 2004.
[27] S. Cheng, M. C. Valenti, and D. Torrieri, "Turbo-NFSK: Iterative estimation, noncoherent demodulation, and decoding for fast fading channels," in Proc. IEEE Military Commun. Conf. (MILCOM), Atlantic City, NJ, Nov. 2005, to be published.

Matthew C. Valenti (M'99) received the B.S.E.E. degree from Virginia Polytechnic Institute and State University (Virginia Tech), Blacksburg, in 1992, the M.S.E.E. degree from The Johns Hopkins University, Baltimore, MD, in 1995, and the Ph.D. degree in electrical engineering from Virginia Tech, in 1999, where he was a Bradley Fellow.

He is currently an Associate Professor in the Lane Department of Computer Science and Electrical Engineering, West Virginia University, Morgantown. He also acts as a consultant to several companies engaged in various aspects of turbo and LDPC codec design, including software radio, FPGA, and ASIC implementations for military, satellite, and third-generation cellular applications. Prior to attending graduate school at Virginia Tech, he was an Electronics Engineer at the United States Naval Research Laboratory, Washington, DC. He has been on the technical program committee for several international conferences. His research interests are in the areas of communication theory, error correction coding, applied information theory, and wireless multiple-access networks.

Dr. Valenti serves as an Associate Editor for the IEEE TRANSACTIONS ON VEHICULAR TECHNOLOGY.

Shi Cheng (S'01) received the B.E. and M.S. degrees in electrical engineering from Southeast University, Nanjing, China, in 2000 and 2003, respectively. He is currently working towards the Ph.D. degree in electrical engineering at West Virginia University, Morgantown.

From 2000 to 2003, he was a Research Assistant with the Digital Signal Processing Laboratory, Southeast University, Nanjing, China. His current research interests are error correction coding and wireless communication systems.